J Arid Land (2023) 15(9): 1023–1036
https://doi.org/10.1007/s40333-023-0063-y

Science Press Springer-Verlag

Projecting future precipitation change across the semi-arid Borana lowland, southern Ethiopia

Mitiku A WORKU[1*], Gudina L FEYISA[2], Kassahun T BEKETIE[2], Emmanuel GARBOLINO[3]

[1] Department of Environment and Climate Change Management, Ethiopian Civil Service University, Addis Ababa 1000, Ethiopia;
[2] Center for Environmental Science, Addis Ababa University, Addis Ababa 1000, Ethiopia;
[3] Climpact Data Science, Nova-Sophia 06904, France

Abstract: Climate change caused by past, current, and future greenhouse gas emissions has become a major concern for scientists in the field in many countries and regions of the world. This study modelled future precipitation change by downscaling a set of large-scale climate predictor variables (predictors) from the second generation Canadian Earth System Model (CanESM2) under two Representative Concentration Pathway (RCP) emission scenarios (RCP4.5 and RCP8.5) in the semi-arid Borana lowland, southern Ethiopia. The Statistical DownScaling Model (SDSM) 4.2.9 was employed to downscale and project future precipitation change in the middle (2036–2065; 2050s) and far (2066–2095; 2080s) future at the local scale. Historical precipitation observations from eight meteorological stations stretching from 1981 to 1995 and 1996 to 2005 were used for the model calibration and validation, respectively, and the time period of 1981–2018 was considered and used as the baseline period to analyze future precipitation change. The results revealed that the surface-specific humidity and the geopotential height at 500 hPa were the preferred large-scale predictors. Compared to the middle future (2050s), precipitation showed a much greater increase in the far future (2080s) under both RCP4.5 and RCP8.5 scenarios at all meteorological stations (except Teletele and Dillo stations). At Teltele station, the projected annual precipitation will decrease by 26.53% (2050s) and 39.45% (2080s) under RCP4.5 scenario, and 34.99% (2050s) and 60.62% (2080s) under RCP8.5 scenario. Seasonally, the main rainy period would shift from spring (March to May) to autumn (September to November) at Dehas, Dire, Moyale, and Teltele stations, but for Arero and Yabelo stations, spring would consistently receive more precipitation than autumn. It can be concluded that future precipitation in the semi-arid Borana lowland is predicted to differ under the two climate scenarios (RCP4.5 and RCP8.5), showing an increasing trend at most meteorological stations. This information could be helpful for policymakers to design adaptation plans in water resources management, and we suggest that the government should give more attention to improve early warning systems in drought-prone areas by providing dependable climate forecast information as early as possible.

Keywords: future precipitation; climate change; second generation Canadian Earth System Model (CanESM2); Statistical DownScaling Model (SDSM); semi-arid Borana lowland; southern Ethiopia

Citation: Mitiku A WORKU, Gudina L FEYISA, Kassahun T BEKETIE, Emmanuel GARBOLINO. 2023. Projecting future precipitation change across the semi-arid Borana lowland, southern Ethiopia. Journal of Arid Land, 15(9): 1023–1036. https://doi.org/10.1007/s40333-023-0063-y

1 Introduction

Strong evidence has suggested that global climate is changing mainly as a result of the increasing

*Corresponding author: Mitiku A WORKU (E-mail: adismite2011@gmail.com)
Received 2022-12-14; revised 2023-06-14; accepted 2023-06-23

concentration of greenhouse gases in the atmosphere emitted from various human activities (Intergovernmental Panel on Climate Change (IPCC), 2014, 2022). The global average temperature showed a warming trend of 0.85°C from 1880 to 2012 (IPCC, 2013; Birara et al., 2018). Moreover, the Fifth Assessment Report of IPCC (IPCC AR5) mentioned that observations including the increase in global average land and sea temperatures, widespread melting of snow and ice, and rising sea level indicate further warming of the climate system (IPCC, 2014).

Human-induced climate change, including more frequent and intense extreme events, has widespread adverse impacts and caused related losses and damages to the physical environment and humans, beyond the natural climate variation. Increase in weather and climate extremes has led to some irreversible impacts since natural and human systems are pushed beyond their adaptive capacity (IPCC, 2022). The vulnerability of ecosystems and humans to climate change differs substantially among different climatic regions, communities, and countries, which can be attributed to socio-economic, cultural, political, governance and geographical factors (Gumucio et al., 2020; IPCC, 2022).

Climate change caused by past, current, and future greenhouse gas emissions has various adverse impacts on the physical environment as well as the socio-economic development of nations (IPCC, 2022), which therefore has become a major concern for scientists in the field (Mekonnen and Berlie, 2020; Bulti et al., 2021). For instance, several studies have proved future increase in the intensity and frequency of extreme events (particularly floods and droughts) until the end of this century in many regions of the world, including Ethiopia (IPCC, 2014; Nasim et al., 2016; Mubeen et al., 2020). Hence, prior information on the future climate is crucial and will play a significant role in identifying potential associated risks at an early stage and supporting the planning and undertaking of intervention measures, including adaptation and mitigation responses, to cope with increasing extreme events.

Climate information for the future period can be projected from Global Circulation Models (GCMs), which are now readily available from different sources but at a coarser resolution (Deb et al., 2018; Bulti et al., 2021). However, the local-scale climate studies demand climate information at a high resolution (fine-scale) (Pervez and Henebry, 2014); hence, scientists came up with the idea of the downscaling method. Among the existing downscaling methods, the statistical downscaling that assumes the empirical relationship between the large-scale climatic variables (predictors) and the local-scale variable (predictand) has been widely adopted (Wilby et al., 2002; Wilby and Dawson, 2013). Despite its limitation, statistical downscaling can provide the first-hand information about the future climate condition.

Arid and semi-arid areas in the Sahel region and the Horn of Africa are often identified as the most vulnerable regions, where pastoralists, fishing communities, and small-holder farmers are adversely impacted by the current and future climate (Ayanlade and Ojebisi, 2019; Muringai et al., 2019; Mogomotsi et al., 2020; IPCC, 2022). Climate change has already negatively impacted crop production by altering the pattern and distribution of precipitation (Sultan et al., 2019) and has reduced the total agricultural productivity growth by 34% in Africa since 1961 (Ortiz-Bobea et al., 2021). Impacts of global climate on food availability are expected to lead to higher food prices and greater risk of hunger for people in African countries, including the semi-arid lowlands of Ethiopia (IPCC, 2022). Previous research on the projection of future climate change at the local scale by downscaling of the GCMs (Hussain et al., 2017; Matthew and Abiye, 2017; Hasan and Nile, 2020; Mohammed et al., 2020; Bulti et al., 2021; Javaherian et al., 2021; Seng et al., 2021; Shahriar et al., 2021; Tarekegn et al., 2021; Munawar et al., 2022) was conducted either in highland regions where precipitation is not scarce or at the larger spatial scales that make local-scale climate analysis still a challenging issue. Thus, it is interesting to study precipitation change at the station or district scale, which helps to identify the areas with limited precipitation conditions and provide information to suggest better management practices.

From this perspective, in this paper, we chose the semi-arid Borana lowland, one of the semi-arid regions that is frequently hit by extreme climate conditions in Ethiopia, particularly drought, as a case study. There is a need to obtain prior climate information in this region to help

manage the drought-related risks through various mechanisms. Besides, studies on the future precipitation change in the semi-arid Borana lowland can also provide support information to decision-makers, local institutions, and inhabitants that exclusively engaged in climate-sensitive sectors such as livestock systems and small-holder farming. Based on this, we projected future precipitation change in the middle future (2036–2065; 2050s) and far future (2066–2095; 2080s) through downscaling of the second generation Canadian Earth System Model (CanESM2) GCM data under two Representative Concentration Pathway (RCP) emission scenarios (RCP4.5 and RCP8.5) in the semi-arid Borana lowland of southern Ethiopia. The research findings will help to formulate better measures for water resources management and reduce the adverse effects of climate-related risks in the locality.

2 Materials and methods

2.1 Study area

The semi-arid Borana lowland (103°03′–103°05′E, 03°30′–05°38′N; 450–2487 m a.s.l.) is located in the southern part of Ethiopia (Fig. 1). The annual mean temperature varies between 28°C and 33°C with little seasonal variation (Fenetahun et al., 2022), and the mean annual precipitation was estimated between 350 and 900 mm by Debela et al. (2019) and between 285 and 741 mm by Worku et al. (2022). Precipitation with high spatial and temporal fluctuations falls mainly during two periods: spring (from March to May) and autumn (from September to November), which accounts for nearly 60% and 27% of annual precipitation, respectively (Gemedo et al., 2006). There are two dry seasons in the study area, including the long dry spell in winter (from December to February of the next year) and the short dry spell in summer (from June to August) (Korecha and Barnston, 2007). The seasonal characteristics of the study area as well as the pattern and distribution of precipitation are unique and differ from those of other regions in Ethiopia. In summer, when the most regions of Ethiopia receive rain, the semi-arid Borana lowland remains dry due to its rain-shadow location.

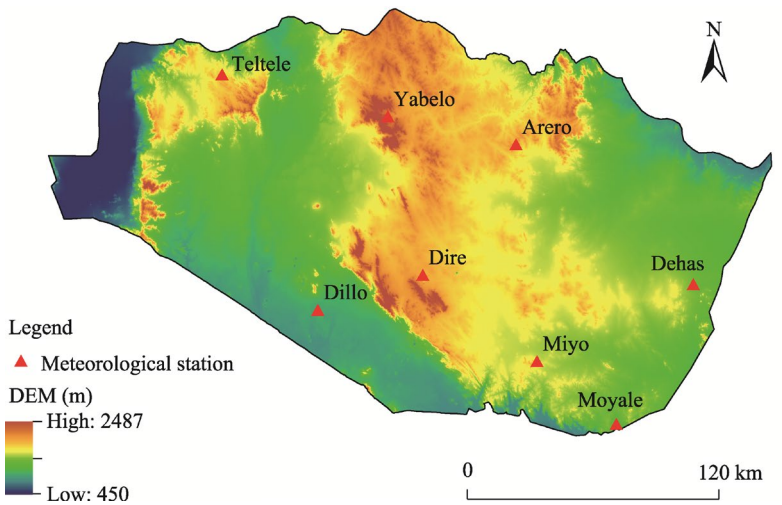

Fig. 1 Overview of the semi-arid Borana lowland based on digital elevation model (DEM) data. The DEM data were downloaded from the United States Geological Survey (USGS) Earth Resources Observation and Science (EROS) Archive-Shuttle Radar Topographic Mission (SRTM) with the spatial resolution of 1 arc-second (https://www.usgs.gov).

2.2 Data sources

2.2.1 Meteorological data

Historical daily precipitation observations stretching from 1981 to 2018 at all meteorological stations in the study area (Fig. 1) were collected from the Ethiopian Meteorological Institute

(EMI) (https://www.ethiomet.gov.et). Since meteorological station observations are not free from missing values, gridded precipitation data with a spatial resolution of 4 km×4 km were used to complete the data. The gridded precipitation data used in this study are a product of Enhancing National Climate Services (ENACTS) initiative that integrates the meteorological station observations with freely available high-resolution global products using Climate Data Tool (CDT) (https://iri.columbia.edu/resources/ enacts/).

2.2.2 CanESM2 GCM

The CanESM2 GCM was developed by the Canadian Centre for Climate Modelling and Analysis (CCCma), which is freely available online (https://www.climate-scenarios.canada.ca). It is a comprehensive earth system model that includes coupled atmosphere, ocean, sea-ice, and terrestrial and ocean carbon components (Arora et al., 2011; Virgin et al., 2021; Jeong et al., 2022), with a resolution of 2.8125° latitude×2.8125° longitude (Arora et al., 2011). CanESM2 GCM has been widely applied in Ethiopia (Dile et al., 2013; Deb et al., 2018; Bulti et al., 2021; Tarekegn et al., 2021) and other tropical regions (Javaherian et al., 2021; Seng et al., 2021; Shahriar et al., 2021; Lachgar et al., 2022).

The particular ensemble used in the CanESM2 GCM is the first member team where the past climate condition over the period of 1961–2005 is represented by historical simulation. Projections for future climate are based on the scenarios in the IPCC AR5 and hence the projected time period by this model is from 2006 to 2100. We downloaded 26 climate variables from the CanESM2 GCM data for both historical period (1961–2005) and future period (2006–2100) under RCP4.5 and RCP8.5 scenarios. These data were ready to be used as inputs in the statistical downscaling models and to further obtain the downscaled future precipitation data of the semi-arid Borana lowland.

2.2.3 National Center for Environmental Prediction/National Center for Atmospheric Research (NCEP/NCAR) reanalysis dataset

The reanalysis dataset for the large-scale climate variables during 1961–2005 was obtained from the NCEP/NCAR with a horizontal resolution of 2.5000° latitude×2.5000° longitude (Goyal and Ojha, 2012). The NCEP/NCAR dataset was used for the calibration and validation of the downscaling model in this study. We chose the grid data that fall in BOX_015X_34Y (where 015 is the longitudinal index and 34 is the latitudinal index) and interpolated them to adjust the resolution to be the same as CanESM2 GCM data. Then, all of these climate variables were normalized using the following equation (Hassan et al., 2014; Bulti et al., 2021; Shahriar et al., 2021):

$$\hat{u} = \frac{u_t - \overline{u}}{\sigma_u}, \tag{1}$$

where $\hat{u}$ is the normalized value for the climate variable at time t; u_t is the original value for the climate variable at time t; $\overline{u}$ is the multi-year average value for the climate variable over the period; and σ_u is the standard deviation.

2.3 Statistical DownsSaling Model (SDSM)

2.3.1 Model setup

The SDSM is a regression-based hybrid model that combines stochastic weather generation and multiple linear regression (MLR) for generating future emission scenarios (Wilby et al., 2002). In this study, we used the SDSM 4.2.9 to downscale and project future precipitation. The SDSM in the first place calculates the relationship between the large-scale predictors and the local-scale predictand to develop future climate conditions. There are two sub-models in the SDSM, namely conditional and unconditional processes, where the conditional sub-model is used for precipitation projection since it is dependent on other factors (i.e., predictors) (Wilby et al., 2002). The SDSM is performed by taking into account the steps, including the screening of predictors, the calibration and validation of the model, and the generation of climate scenarios. The model structure is described in Figure 2 (Wilby et al., 2002; Hasan and Nile, 2020; Shahriar et al., 2021).

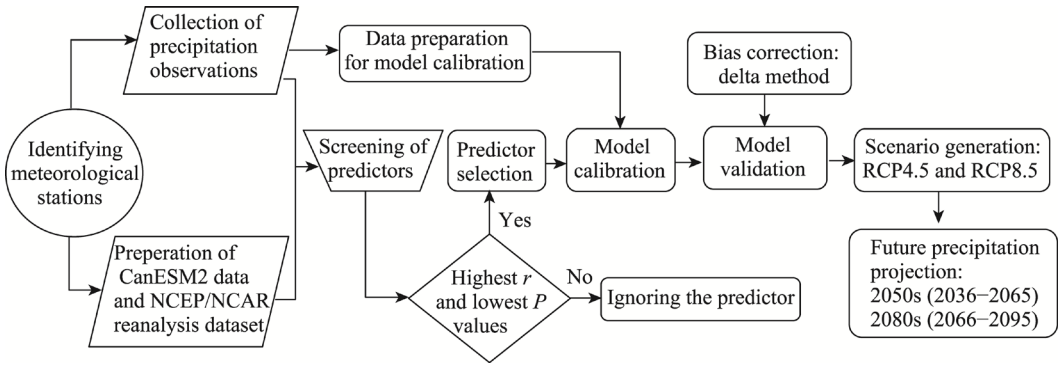

Fig. 2 Statistical DownScaling Model (SDSM) structure used in this study. CanESM2, second generation Canadian Earth System Model; NCEP/NCAR, National Center for Environmental Prediction/National Center for Atmospheric Research; RCP, Representative Concentration Pathway. *r* represents the correlation coefficient, and *P* represents the statistical significance.

2.3.2 Selection of appropriate large-scale predictors

Appropriate selection of large-scale climate variables (termed as predictors) is most important in the projection of future precipitation, since it highly affects the future climate scenarios (Hassan and Nile, 2020). The screening of predictors was then adopted by taking into account different approaches, including the results of a correlation coefficient matrix, partial correlation, scatter plots, and *P*-value among the observed precipitation and the NCEP/NCAR predictors. To this end, a relatively high correlation coefficient (r>0.6) and a low *P*-value (P<0.05) were used to select the best predictors (Yang et al., 2017; Ozbuldu and Irvem, 2021). The entire NCEP/NCAR predictors are given in Table 1.

Table 1 List of the large-scale predictors in the NCEP/NCAR reanalysis dataset and CanESM2 GCM

No.	Predictor	Description	No.	Predictor	Description
1	mslp	Mean sea level pressure	14	p5zh	Divergence at 500 hPa
2	p1_f	Geostrophic air flow velocity at surface	15	p8_f	Geostrophic air flow velocity at 850 hPa
3	p1_u	Zonal velocity component at surface	16	p8_u	Zonal velocity component at 850 hPa
4	p1_v	Meridional velocity component at surface	17	p8_v	Meridional velocity component at 850 hPa
5	p1_z	Vorticity at surface	18	p8_z	Vorticity at 850 hPa
6	p1th	Wind direction at surface	19	p850	850 hPa geopotential height
7	p1zh	Divergence at surface	20	p8th	Wind direction at 850 hPa
8	p5_f	Geostrophic air flow velocity at 500 hPa	21	p8zh	Divergence at 850 hPa
9	p5_u	Zonal velocity component at 500 hPa	22	prcp	Total precipitation
10	p5_v	Meridional velocity component at 500 hPa	23	s500	Specific humidity at 500 hPa
11	p5_z	Vorticity at 500 hPa	24	s850	Specific humidity at 850 hPa
12	p500	Geopotential height at 500 hPa	25	shum	Surface-specific humidity
13	p5th	Wind direction at 500 hPa	26	temp	Mean temperature at 2 m

Note: NCEP/NCAR, National Center for Environmental Prediction/National Center for Atmospheric Research; CanESM2, second generation Canadian Earth System Model; GCM, Global Circulation Model.

2.3.3 Calibration and validation of the SDSM

Following the selection of the large-scale predictors, the final ones were used in the calibration of the SDSM. At this time, a multiple regression equation with the optimization techniques of the ordinary least squares (OLS) method was used to derive the relationship between the large-scale predictors and the local-scale predictand (Shahriar et al., 2021). Based on the available historical daily precipitation observations (1981–2018), we classified the data into two sets: precipitation observations stretching from 1981 to 1995 for the calibration of the SDSM; and precipitation observations stretching from 1996 to 2005 for the validation of the SDSM.

The model performance was evaluated using the coefficient of determination (R^2) and the root means square error (RMSE) by the following equations (Hu et al., 2016; Mathew and Abiye, 2017; Habib ur Rahman et al., 2018; Mubeen et al., 2020; Javaherian et al., 2021):

$$R^2=\frac{\sum_{i=1}^{n}(P_i-\overline{P})(O_i-\overline{O})}{\sqrt{\sum_{i=1}^{n}(P_i-\overline{P})^2\sum_{i=1}^{n}(O_i-\overline{O})^2}}, \tag{2}$$

$$\mathrm{RMSE}=\sqrt{\frac{1}{n}\sum_{i=1}^{n}(P_i-O_i)^2}, \tag{3}$$

where, P_i is the projected daily precipitation (mm); O_i is the observed daily precipitation (mm); $\overline{P}$ and $\overline{O}$ are the average of projected daily precipitation (mm) and average of observed daily precipitation (mm), respectively; and n represents the total number of data. The closer the R^2 value to 1 and the RMSE value to 0, the better the projection for future precipitation will be (Ghorbani et al., 2018). The calibrated and validated results are provided in Table 2.

Table 2 Statistical indices for the calibration and validation of the SDSM

Station	Calibration period (1981–1995)		Validation period (1996–2005)	
	R^2	RMSE	R^2	RMSE
Arero	0.543	1.736	0.653	4.287
Dehas	0.739	1.478	0.500	2.573
Dillo	0.538	2.694	0.493	0.853
Dire	0.690	2.844	0.617	3.198
Miyo	0.771	1.361	0.582	3.122
Moyale	0.580	0.049	0.480	4.886
Teltele	0.601	5.415	0.897	0.525
Yabelo	0.668	1.785	0.604	3.871

Note: SDSM, Statistical DownScaling Model; R^2, coefficient of determination; RMSE, root means square error.

2.3.4 Bias correction

To remove the errors in the downscaled precipitation, bias correction is necessary (Wilby and Dawson, 2013; Hussain et al., 2017; Shahriar et al., 2021). We adopted delta method to eliminate the overestimation and/or underestimation of the model outputs from the daily time series of the downscaled precipitation. The equation is given by Dessu and Melesse (2013):

$$P_{\mathrm{deb}}=P_{\mathrm{scen\ (daily)}}\times\left(\frac{\overline{P}_{\mathrm{obs\ (monthly)}}}{\overline{P}_{\mathrm{cont\ (monthly)}}}\right), \tag{4}$$

where, P_{deb} is the de-biased (corrected) daily precipitation (mm) for future time period; $P_{\mathrm{scen\ (daily)}}$ is the daily precipitation generated by the SDSM for the future time period (mm); $\overline{P}_{\mathrm{cont\ (monthly)}}$ is the mean monthly precipitation for the baseline period (1981–2018) simulated by the SDSM (mm); and $\overline{P}_{\mathrm{obs\ (monthly)}}$ represents the mean monthly precipitation observed in the baseline period (1981–2018) (mm). It should be noted that the time period of 1981–2018 was considered and used as the baseline period to analyze future precipitation change in the study area.

2.3.5 Generation of future climate scenarios

After bias correction, future climate scenarios were generated for the middle (2050s) and far (2080s) future. Among the four different emission scenarios (RCP2.6, RCP4.5, RCP6.0, and RCP8.5) developed by the CanESM2 (Moss et al., 2010; Meinshausen et al., 2011; van Vuuren et al., 2011; IPCC, 2013), the RCP4.5 scenario (characterized by limited mitigation practices with the radiative forcing of 4.5 W/m^2 by 2100) and RCP8.5 scenario (with no mitigation practices

implemented and ultimately resulting in a radiative forcing of 8.5 W/m^2 by 2100), were considered in the study. The RCP2.6 scenario is a 'peak-and-decline' scenario that will lead to very low greenhouse gas concentration levels whereby the radiative forcing will reach up to 3.0 W/m^2 by 2050 and return to 2.6 W/m^2 by 2100 (van Vuuren et al., 2011). Due to its stringent mitigation strategy, the RCP2.6 scenario was overlooked in this paper. In addition, the RCP6.0 scenario which falls between the limited and no mitigation strategies in the future was not considered.

3 Results

3.1 Selection of appropriate large-scale predictors

The NCEP/NCAR predictors were evaluated against each other using correlation coefficient and *P*-value. Accordingly, the surface-specific humidity presented the most important large-scale predictor for the predictand (precipitation) followed by the geopotential height at 500 hPa (Table 3). Apart from these, the geopotential height at 850 hPa projected local-scale precipitation very well at three meteorological stations, while both the geostrophic air flow velocity at 850 hPa and mean temperature at 2 m projected local-scale precipitation well at two meteorological stations in the study area (Table 3).

Table 3 NCEP/NCAR predictors screened out to downscale precipitation in the SDSM

Station	Predictand	Predictor							
		mslp	p500	p8_f	p8_u	p850	p8zh	shum	temp
Arero	Precipitation		√	√		√			
Dehas	Precipitation		√					√	
Dillo	Precipitation			√	√			√	
Dire	Precipitation	√	√					√	
Miyo	Precipitation						√	√	
Moyale	Precipitation		√			√		√	
Teltele	Precipitation					√		√	√
Yabelo	Precipitation		√					√	√

Note: √ indicates the selected large-scale predictor for precipitation at the corresponding meteorological station.

3.2 Projected monthly precipitation under RCP scenarios

At Arero station, the projected monthly precipitation values were higher than the monthly precipitation observations in the baseline period (1981–2018) (historical observations) (Fig. 3). Specifically, RCP4.5 scenario projected higher precipitation than RCP8.5 scenario in the 2080s in November, October, and April, and the projected precipitation values in the 2080s seemed to be higher than those in the 2050s. The projected precipitation values under RCP4.5 scenario in the 2050s during the main rainy season (March to May) were more or less equal to the historical observations at Dehas station, whereas in the short rainy season (September to November), the projected precipitation values under both scenarios (RCP4.5 and RCP8.5) was higher than the historical observations in the baseline period, particularly in October and November. Unlike other meteorological stations, the monthly projected precipitation values were close to the monthly historical observations at Dillo station, which is also the driest station historically as the models' outputs revealed.

At Dire station, the projected monthly precipitation values in the future were lower than the historical observations in the baseline period only in March and April. In addition, both RCP4.5 and RCP8.5 scenarios projected higher precipitation totals in the middle and far future during the short rainy season than during the main rainy season. The projected monthly precipitation also identified the occurrence of precipitation in June. During all months except for October and November, similar precipitation conditions were observed between the projected values under both RCP4.5 and RCP8.5 scenarios and the historical observations, with the historical

observations slightly lower than the projected ones.

At Moyale station, the projected monthly precipitation values were higher than the monthly historical observations for all months, except for July under RCP8.5 scenario in the far future. Both RCP4.5 and RCP8.5 scenarios projected higher monthly precipitation in October, November, and April, with the values of 370, 210, and 165 mm under RCP8.5 scenario. It seemed that the main rainy season would shift from spring to autumn at most meteorological stations in the future. The projected monthly precipitation values seemed to be lower than the historical observations from March to May at Teltele station; however, both RCP4.5 and RCP8.5 scenarios simulated similar precipitation conditions, except for RCP8.5 scenario in the far future (2080s). Moreover, the projected monthly precipitation revealed drier conditions at Teltele station with no occurrence of precipitation from June to August.

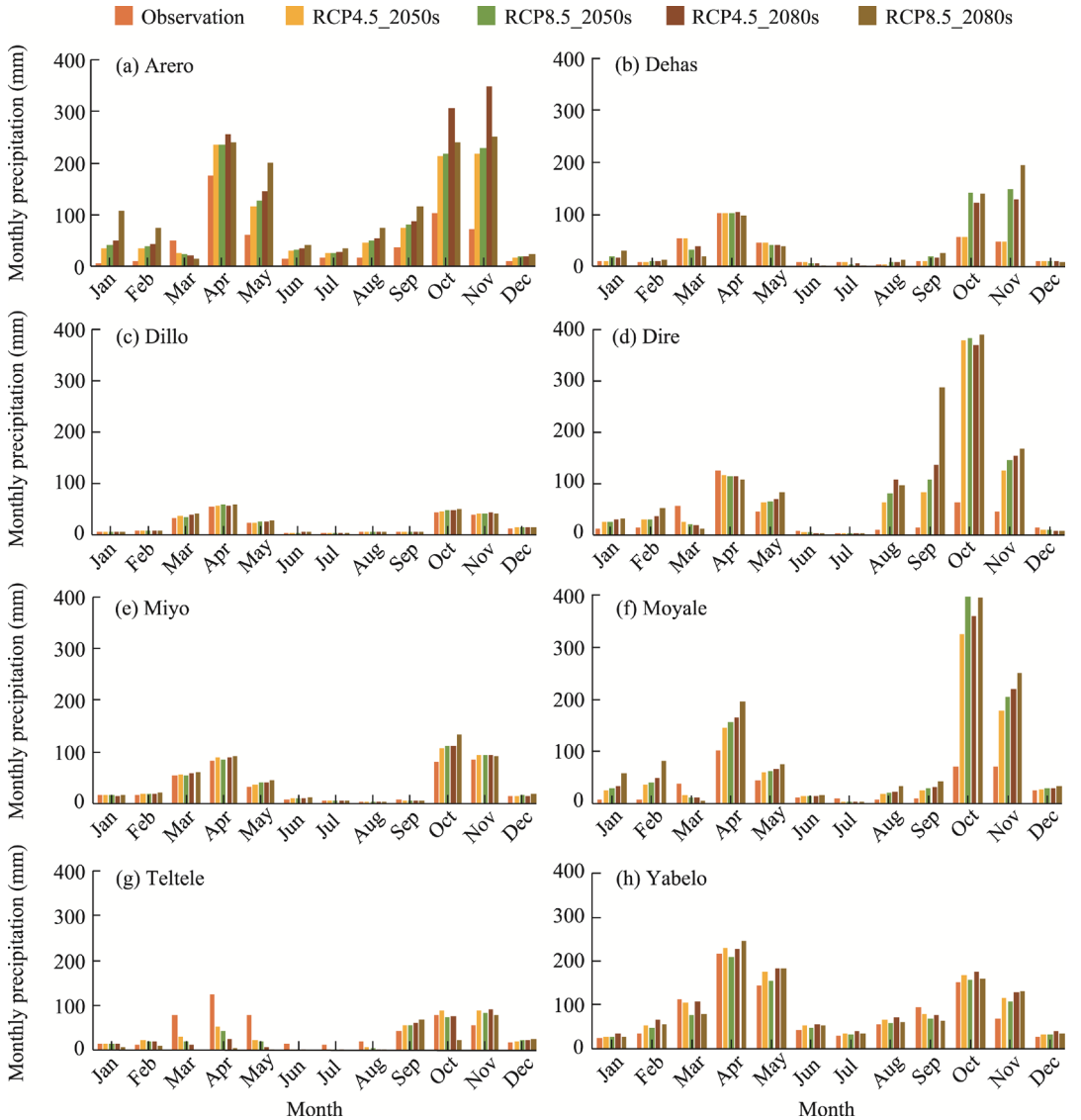

Fig. 3 Projected monthly precipitation from downscaled CanESM2 GCM under RCP4.5 and RCP8.5 scenarios in the middle future (2050s; RCP4.5_2050s and RCP8.5_2050s) and far future (2080s; RCP4.5_2080s and RCP8.5_2080s) compared to the monthly precipitation observations in the baseline period (1981–2018) at the eight meteorological stations. (a), Arero; (b), Dehas; (c), Dillo; (d), Dire; (e), Miyo; (f), Moyale; (g), Teltele; (h), Yabelo.

At Yabelo station, the projected monthly precipitation values were lower than the monthly historical observations only in March and September. Furthermore, the projected monthly precipitation values during the main rainy season were higher than those during the short rainy season under both RCP4.5 and RCP8.5 scenarios at this station.

3.3 Projected seasonal precipitation under RCP scenarios

Concerning the distribution of precipitation in different seasons, it is known that the study area receives much of its precipitation in spring, which is supposed to be the main rainy season, followed by autumn, which is considered as the short rainy season.

As shown in Figure 4, the model projected that spring and summer were expected to receive more precipitation than autumn in the middle and far future at Arero station. The projected seasonal results also revealed that more precipitation would occur in autumn at Dehas, Dire, Moyale, and Teltele stations. At Teltele station particularly, the projected seasonal precipitation fell below the historical observations, whereas it showed some similarity with the historical observations at Yabelo station; furthermore, more precipitation would occur in spring, followed by autumn at this station.

At more than half of the studied meteorological stations, the amount of precipitation received in autumn was higher than that in spring. Overall, it can be summarized that, in the future (both middle and far future), there will be a shift in the main rainy season from spring to autumn. This means that precipitation in autumn will be more than that in spring, which will exert a greater impact on the socio-economic activities in the study area in the future.

3.4 Projected annual precipitation under RCP scenarios

The projected annual precipitation values under two scenarios in the future (middle and far future) were compared to the precipitation observations in the baseline period (1981–2018) for all meteorological stations in the study area (Table 4). The results revealed that both RCP4.5 and RCP8.5 scenarios projected a huge increase in annual precipitation in the far future (2080s), compared to the middle future (2050s). Moreover, a significant disparity can be observed among meteorological stations, where Arero, Dire, and Moyale stations exhibited the higher increases in annual precipitation in the future, compared to other meteorological stations.

At Teltele station, the projected values for annual precipitation were lower than the historical observations, with decreases of 26.53% (2050s) and 39.45% (2080s) under RCP4.5 scenario, and 34.99% (2050s) and 60.62% (2080s) under RCP8.5 scenario. Hence, drier conditions will occur in the future for this station. Similar results appeared at Dillo station, with decreases of 2.26% (RCP4.5 scenario) and 1.07% (RCP8.5 scenario) in the middle future (2050s).

On the other hand, the projected annual precipitation exhibited increases of 13.42% (Miyo station) and 119.76% (Moyale station) under RCP4.5 scenario in the middle future, and 0.80% (Dillo station) and 154.65% (Dire station) under RCP4.5 scenario in the far future. In addition, under RCP8.5 scenario, we observed percentage changes from 2.10% (Yabelo station) to 150.62% (Moyale station) and from 3.20% (Dillo station) to 200.69% (Dire station) in the middle and far future, respectively. Accordingly, Moyale and Dire stations will experience a significant increase in annual precipitation in the future, compared to other meteorological stations.

4 Discussion

The large-scale predictors of the surface-specific humidity and geopotential height at 500 hPa projected local-scale precipitation well at seven and five of the eight meteorological stations, respectively. Similarly, Bulti et al. (2021) found that the surface-specific humidity is one of the super predictors of CanESM2 in analyzing future extreme precipitation in Adama, Ethiopia. On the other hand, the total precipitation was reported as the super predictor at Kuching, Bintulu, and Limbang stations, while the geopotential height at 500 hPa projected the minimum temperature well at Bintulu and Limbang stations in Chittagong Division, Bangladesh (Hussain et al., 2017).

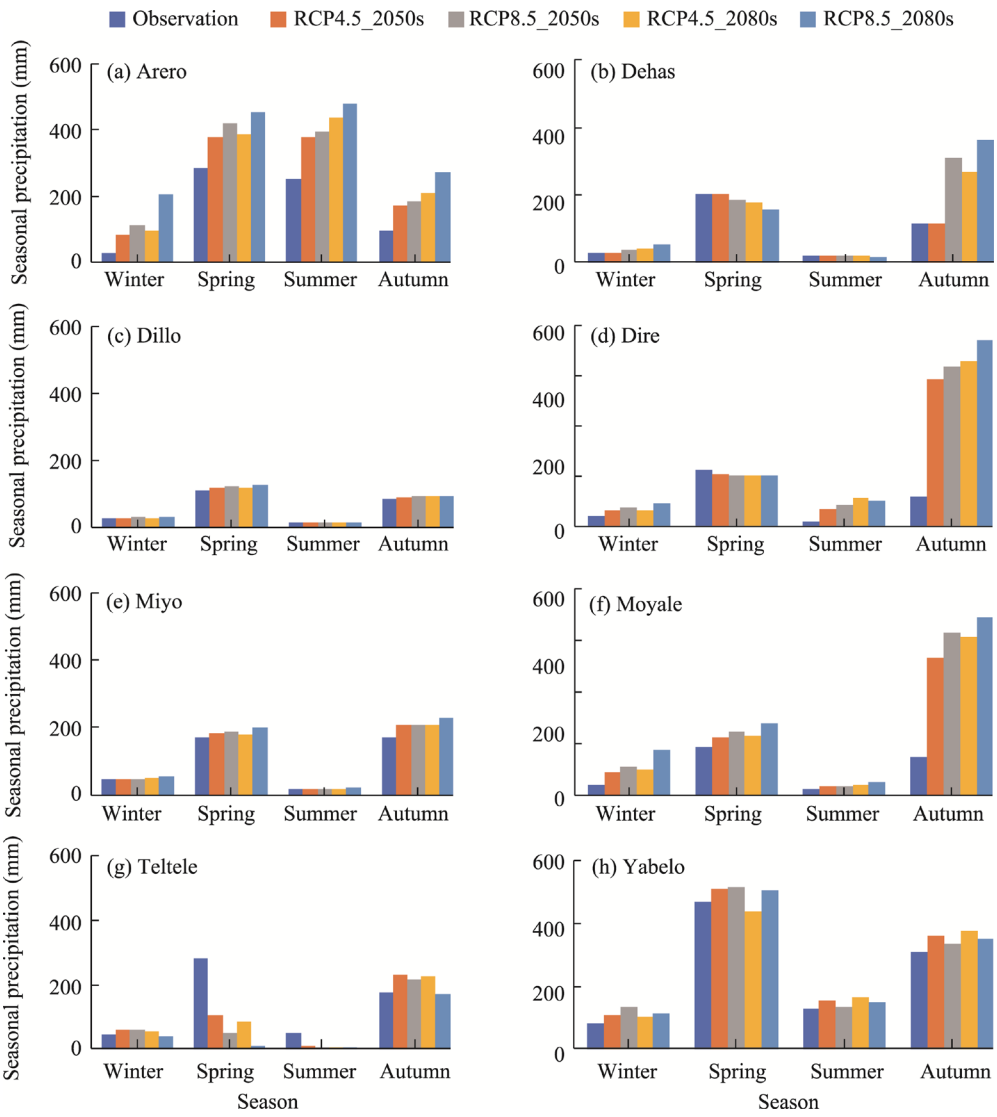

Fig. 4 Projected seasonal precipitation from downscaled CanESM2 GCM under RCP4.5 and RCP8.5 scenarios in the middle future (2050s; RCP4.5_2050s and RCP8.5_2050s) and far future (2080s; RCP4.5_2080s and RCP8.5_2080s) compared to the seasonal precipitation observations in the baseline period (1981–2018) at the eight meteorological stations. (a), Arero; (b), Dehas; (c), Dillo; (d), Dire; (e), Miyo; (f), Moyale; (g), Teltele; (h), Yabelo.

Table 4 Percentage change of projected annual precipitation in the middle (2050s) and far (2080s) future compared to the precipitation observations in the baseline period (1981–2018) at the eight meteorological stations

Climate scenario	Percentage change of projected annual precipitation (%)							
	Arero	Dehas	Dillo	Dire	Miyo	Moyale	Teltele	Yabelo
RCP4.5_2050s	85.38	30.27	–2.26	124.63	13.42	119.76	–26.53	14.36
RCP4.5_2080s	141.94	40.07	0.80	154.65	14.69	153.48	–39.45	20.68
RCP8.5_2050s	94.76	48.68	–1.07	140.41	13.22	150.62	–34.99	2.10
RCP8.5_2080s	145.97	61.18	3.20	200.69	24.64	199.62	–60.62	12.64

Note: RCP, Representative Concentration Pathway. RCP4.5_2050s and RCP8.5_2050s indicate RCP4.5 and RCP8.5 scenarios in the middle future; RCP4.5_2080s and RCP8.5_2080s indicate RCP4.5 and RCP8.5 scenarios in the far future.

According to Matthew and Abiye (2017), the mean sea level pressure, geostrophic air flow velocity at surface, surface-specific humidity, and specific humidity at 500 hPa were the most sensitive large-scale predictors for projecting future local-scale precipitation over Nigeria. The selection of the large-scale predictors in this study was mostly similar to the procedures applied in Hashmi et al. (2011), Hassan et al. (2014), and Hussain et al. (2017).

The study area has been one of the driest regions in Ethiopia in winter and summer in the past. It is consistent with the situation in the future because the model projected drier conditions at meteorological stations including Dehas, Dillo, Dire, Miyo, and Teltele. Months from December to February of the next year are getting drier over the whole country due to the invasion of dry continental winds from Asian landmasses and northern Africa. The influence of these winds will be sustained even in the future and become responsible for the extended dryness in this region. However, during the months from June to August, most parts of the country will receive more precipitation with the exceptions of the study area and the northeastern lowlands of Ethiopia, which can be attributed to their rain-shadow locations in summer. Similar conditions were projected under RCP4.5 and RCP8.5 scenarios in the middle (2050s) and far (2080s) future.

Precipitation from March to May was projected to decrease in the future in the study area, particularly at stations of Dillo, Miyo, and Teltele, whereas more precipitation will occur in October and November than in other months at Dehas, Dire, and Moyale stations. Therefore, the distribution of projected monthly precipitation will not be consistent over the semi-arid Borana lowland. According to Tarekegn et al. (2022), the simulated monthly precipitation exhibited a decreasing trend in all months in the 2050s and 2080s, with the highest decrease (97.00%) under RCP8.5 scenario in the 2050s. In addition, Mohammed et al. (2020) found a decrease in future precipitation in February, April, and June under both RCP4.5 and RCP8.5 scenarios, where the highest decrease was projected in February in the 2080s (45.00% and 43.40% under RCP4.5 and RCP8.5 scenarios, respectively), in the Rift Valley Basin, Ethiopia.

In this study, the projected seasonal precipitation was not consistent across the meteorological stations in the Borana lowland. Except for Arero station, summer was projected to be the driest season in the study area under both RCP4.5 and RCP8.5 scenarios. This was supported by the research of Javaherian et al. (2021), who reported the lowest precipitation in summer at Lar Dam, Iran. At Dehas, Dire, Miyo, Moyale, and Teltele stations, the higher precipitation in the future was projected in autumn and similar result was obtained by Javaherian et al. (2021). Some meteorological stations, including Arero, Dillo, and Yabelo, would obtain more precipitation in spring, which was consistent with the results of Mohammed et al. (2020), who found that future precipitation will increase by 16.00% (RCP4.5 scenario) and 20.00% (RCP8.5 scenario) in spring in the 2080s. Dille et al. (2013) also found increasing trends of spring precipitation in the 2050s and 2080s in the Gilgel Abay River Basin, Ethiopia. Winter followed by summer will be drier seasons across the study area, as revealed in this study. As reported by Mohammed et al. (2020), future precipitation in winter will decrease by 1.80% under RCP4.5 scenario in the 2050s. Similarly, Lachgar et al. (2022) also noticed a reduction in future precipitation in winter and summer over Casablanca City, Morocco.

Annual precipitation was projected to increase in the future at most of meteorological stations apart from Teltele and Dillo, which exhibited reductions in annual precipitation in the future. The results of this study were consistent with the research conducted in Tikur Wuha, Adama City, central Ethiopia ((Mohammed et al., 2020; Bulti et al., 2021) and Bilate Watershed, Ethiopian Rift Valley Basin (Tekle, 2015). Mohammed et al. (2020) predicted increases in future precipitation by 15.40% (RCP4.5) and 17.40% (RCP8.5) in the 2050s as well as 16.00% (RCP4.5) and 19.44% (RCP8.5) in the 2080s. On the other hand, contrary to the current study, Tarekegn et al. (2022) found a reduction in mean annual precipitation of about 22.50% in the 2080s, and the reduction under Special Report on Emission Scenarios (SRES; A2 and B2 scenarios) will be greater than it under RCP scenarios (RCP4.5 and RCP8.5). Decreases in annual precipitation of 20.00%–30.00% under RCP4.5 scenario and about 20.00%–40.00% under RCP8.5 scenario were also projected in the Casablanca Settat region of Morocco during the period of 2036–2100 (Lachgar et al., 2022).

5 Conclusions

In this study, we projected future precipitation in the semi-arid Borana lowland of southern Ethiopia under RCP4.5 and RCP8.5 scenarios using the SDSM. We downscaled the CanESM2 GCM data in the middle (2050s) and far (2080s) future and projected future precipitation at the monthly, seasonal, and annual scales.

Based on partial correlation, scatter plots, and *P*-value, the surface-specific humidity and the geopotential height at 500 hPa were screened out as the most prominent predictors among the 26 NCEP/NCAR large-scale predictors for the predictand (precipitation). Both RCP4.5 and RCP8.5 scenarios projected a huge increase in annual precipitation in the far future (2080s) compared to the middle future (2050s), with significant disparity among meteorological stations, where Arero, Dire, and Moyale stations exhibited the higher increases in future precipitation. On the other hand, at Teltele station, the projected annual precipitation will decrease by 26.53% (2050s) and 39.45% (2080s) under RCP4.5 scenario, and 34.99% (2050s) and 60.62% (2080s) under RCP8.5 scenario. There would be an increase in the projected annual precipitation for most of meteorological stations except Teltele and Dillo stations. Seasonally, the projected precipitation in the future would be higher in autumn than in spring at Dehas, Dire, Moyale, and Teltele stations, and there will be a shift of the main rainy season from spring to autumn at these stations. Further, spring would remain the main rainy season at Arero and Yabelo stations in the future. The increases of projected monthly precipitation will be greater in April, March, October and November than in other months.

In general, it can be concluded that future precipitation in the semi-arid Borana lowland will change considerably under RCP4.5 and RCP8.5 scenarios. This study can be a source of information for policymakers to prepare readiness plans and formulate better measures that can help to reduce climate-related risks. Climate modelling is not free from uncertainties, and further downscaling research, involving studies of multi-GCM ensembles and downscaling approaches, could reduce the uncertainties associated with them and produce better performance.

Conflict of interest

The authors declare that they have no known competing financial interests or personal relationships that could have appeared to influence the work reported in this paper.

Acknowledgements

The authors thank the Ethiopian Meteorological Institute for the station and gridded data and the Canadian Centre for Climate Modelling and Analysis (CCCma) for the CanESM2 GCM data used in this study. Special thanks are given to the editors and anonymous reviewers for their constructive comments that help to improve the manuscript.

Author contributions

Conceptualization: Mitiku A WORKU; Methodology: Mitiku A WORKU; Software: Mitiku A WORKU; Formal analysis: Mitiku A WORKU; Writing - original draft preparation: Mitiku A WORKU; Writing - review and editing: Gudina L FEYISA, Kassahun T BEKETIE, Emmanuel GARBOLINO; Resources: Mitiku A WORKU, Gudina L FEYISA, Kassahun T BEKETIE, Emmanuel GARBOLINO; Supervision: Gudina L FEYISA, Kassahun T BEKETIE.

References

Arora V K, Scinocca J F, Boer G J, et al. 2011. Carbon emission limits required to satisfy future representative concentration pathways of greenhouse gases. Geophysical Research Letters, 38(5): L05805, doi: 10.1029/2010GL046270.

Ayanlade A, Ojebisi S M. 2019. Climate change impacts on cattle production: analysis of cattle herders' climate variability/change adaptation strategies in Nigeria. Change and Adaptation in Socio-Ecological Systems, 5(1): 12–23.

Birara H, Pandey R P, Mishra S K. 2018. Trend and variability analysis of rainfall and temperature in the Tana Basin region, Ethiopia. Journal of Water and Climate Change, 9(3): 555–569.

Bulti D T, Abebe B G, Biru Z. 2021. Analysis of the changes in historical and future extreme precipitation under climate change in Adama city, Ethiopia. Modeling Earth Systems and Environment, 7(4): 2575–2587.

Deb P, Babel M S, Denis A F. 2018. Multi-GCMs approach for assessing climate change impact on water resources in Thailand. Modeling Earth Systems and Environment, 4(2): 825–839.

Debela N, McNeil D, Bridle K, et al. 2019. Adaptation to climate change in the pastoral and agropastoral systems of Borana, South Ethiopia: Options and barriers. American Journal of Climate Change, 8(1): 40–60.

Dessu S B, Melesse A M. 2013. Impact and uncertainties of climate change on the hydrology of the Mara River basin, Kenya/Tanzania. Hydrological Processes, 27(20): 2973–2986.

Dile Y T, Berndtsson R, Setegn S G. 2013. Hydrological response to climate change for Gilgel Abay River, in the Lake Tana Basin-Upper Blue Nile Basin of Ethiopia. PLoS ONE, 8(10): e79296, doi: 10.1371/journal.pone.0079296.

Fenetahun Y, Yuan Y, Xu X W, et al. 2022. Borana rangeland of southern Ethiopia: Estimating biomass production and carrying capacity using field and remote sensing data. Plant Diversity, 44(6): 598–606.

Gemedo D, Maass B L, Isselstein J. 2006. Rangeland condition and trend in the semiarid Borana lowlands, southern Oromia, Ethiopia. African Journal of Range & Forage Science, 23(1): 49–58.

Ghorbani M A, Khatibi R, Karimi V, et al. 2018. Learning from multiple models using artificial intelligence to improve model prediction accuracies: Application to river flows. Water Resources Management, 32(13): 4201–4215.

Goyal M K, Ojha C S P. 2012. Downscaling of surface temperature for lake catchment in an arid region in India using linear multiple regression and neural networks. International Journal of Climatology, 32(4): 552–566.

Gumucio T, Hansen J, Huyer S, et al. 2020. Gender-responsive rural climate services: a review of the literature. Climate and Development, 12: 241–254.

Habib ur Rahman M, Ahmada A, Wang X C, et al. 2018. Multi-model projections of future climate and climate change impacts uncertainty assessment for cotton production in Pakistan. Agricultural and Forest Meteorology, 253–254: 94–113.

Hashmi M Z, Shamseldin A Y, Melville B W. 2011. Statistical downscaling of watershed precipitation using gene expression programming (GEP). Environmental Modelling & Software, 26(12): 1639–1646.

Hassan W H, Nile B K. 2020. Climate change and predicting future temperature in Iraq using CanESM2 and HadCM3 modeling. Modeling Earth Systems and Environment, 7(2): 737–748.

Hassan Z, Shamsudin S, Harun S. 2014. Application of SDSM and LARS-WG for simulating and downscaling of rainfall and temperature. Theoretical and Applied Climatology, 116: 243–257.

Hu Z Y, Hu Q, Zhang C, et al. 2016. Evaluation of reanalysis, spatially interpolated and satellite remotely sensed precipitation data sets in Central Asia. Journal of Geophysical Research: Atmospheres, 121(10): 5648–5663.

Hussain M, Yusof K W, Mustafa M R, et al. 2017. Projected changes in temperature and precipitation in Sarawak State of Malaysia for selected CMIP5 climate scenarios. International Journal of Sustainable Development Planning, 12(8): 1299–1311.

IPCC. 2013. Climate Change 2013: The Physical Science Basis. Contribution of Working Group I to the Fifth Assessment Report of the Intergovernmental Panel on Climate Change. Cambridge, United Kingdom and New York, USA: Cambridge University Press.

IPCC. 2014. Climate Change 2014: Mitigation of Climate Change. Contribution of Working Group III to the Fifth Assessment Report of the Intergovernmental Panel on Climate Change. Cambridge, United Kingdom and New York, USA: Cambridge University Press.

IPCC. 2022. Climate Change 2022: Impacts, Adaptation and Vulnerability. Contribution of Working Group II to the Sixth Assessment Report of the Intergovernmental Panel on Climate Change. Cambridge, UK and New York, USA: Cambridge University Press.

Javaherian M, Ebrahimi H, Aminnejad B. 2021. Prediction of changes in climatic parameters using CanESM2 model based on RCP scenarios (case study): Lar dam basin. Ain Shams Engineering Journal, 12(1): 445–454.

Jeong D, Cannon A J, Yu B. 2022. Influences of atmospheric blocking on North American summer heatwaves in a changing climate: a comparison of two Canadian Earth system model large ensembles. Climatic Change, 172(1): 5, doi: 10.1007/s10584-022-03358-3.

Korecha D, Barnston A G. 2007. Predictability of June to September rainfall in Ethiopia. Journal of American Meteorological Society, 135(2): 628–650.

Lachgar R, Badri W, Chlaida M. 2022. Assessment of future changes in downscaled temperature and precipitation over the Casablanca-Settat region (Morocco). Modeling Earth Systems and Environment, 8(2): 2123–2133.

Matthew O J, Abiye O E. 2017. Evaluation of SDSM performance in simulating rainfall and temperature over Nigeria. British Journal of Applied Science & Technology, 20(1): 1–15.

Meinshausen M, Smith S J, Calvin K, et al. 2011. The RCP greenhouse gas concentrations and their extensions from 1765 to 2300. Climatic Change, 109: 213–241.

Mogomotsi P K, Sekelemani A, Mogomotsi G E J. 2020. Climate change adaptation strategies of small-scale farmers in Ngamiland East, Botswana. Climatic Change, 159(3): 441–460.

Mohammed M, Biazn B, Belete M D. 2020. Hydrological impacts of climate change in Tikur Wuha watershed, Ethiopian Rift Valley Basin. Journal of Environment and Earth Science, 10(2): 28–49.

Moss R H, Edmonds J A, Hibbard K A, et al. 2010. The next generation of scenarios for climate change research and assessment. Nature, 463: 747–756.

Mubeen M, Ahmad A, Hammad H M, et al. 2020. Evaluating the climate change impacts on water requirements of cotton-wheat in semi-arid conditions using DSSAT model. Journal of Water and Climate Change, 11(4): 1661–1675.

Munawar S, Rahman G, Moazzam M F U, et al. 2022. Future climate projections using SDSM and LARS-WG downscaling methods for CMIP5 GCMs over the Transboundary Jhelum River Basin of the Himalayas Region. Atmosphere, 13(6): 898, doi: 10.3390/atmos13060898.

Muringai R T, Naidoo D, Mafongoya P, et al. 2019. The impacts of climate change on the livelihood and food security of small-scale fishers in Lake Kariba, Zimbabwe. Journal of Asian and African Studies, 55(2): 298–313.

Nasim W, Belhouchette H, Tariq M, et al. 2016. Correlation studies on nitrogen for sunflower crop across the agroclimatic variability. Environmental Science and Pollution Research, 23(4): 3658–3670.

Ortiz-Bobea A, Ault T R, Carrillo C M, et al. 2021. Anthropogenic climate change has slowed global agricultural productivity growth. Nature Climate Change, 11(4): 306–312.

Ozbuldu M, Irvem A. 2021. Evaluating the effect of the statistical downscaling method on monthly precipitation estimates of global climate models. Global NEST Journal, 23: 1–9.

Pervez S, Henebry G M. 2014. Projections of the Ganges-Brahmaputra precipitation-Downscaled from GCM predictors. Journal of Hydrology, 517: 120–134.

Seng C K, Weng T K, Nakayama A. 2021. Development of statistically downscaled regional climate model based on Representative Concentration Pathways for Ipoh, Subang and KLIA Sepang in Peninsular Malaysia. IOP Conference Series: Earth and Environmental Science, 945: 012022, doi: 10.1088/1755-1315/945/1/012022.

Shahriar S A, Siddique M A M, Rahman S M A. 2021. Climate change projection using statistical downscaling model over Chittagong Division, Bangladesh. Meteorology and Atmospheric Physics, 133: 1409–1427.

Sultan B, Defrance D, Iizumi T. 2019. Evidence of crop production losses in West Africa due to historical global warming in two crop models. Scientific Reports, 9(1): 12834, doi: 10.1038/s41598-019-49167-0.

Tekle A. 2015. Assessment of climate change impact on water availability of Bilate watershed, Ethiopian Rift Valley Basin. In: AFRICON. Addis Ababa, Ethiopia, 1–5, doi: 10.1109/AFRCON.2015.7332041.

van Vuuren D P, Edmonds J, Kainuma M, et al. 2011. The representative concentration pathways: an overview. Climatic Change, 109: 5–31.

Virgin J G, Fletcher C G, Cole J N S, et al. 2021. Cloud feedbacks from CanESM2 to CanESM5.0 and their influence on climate sensitivity. Geoscientific Model Development, 14(9): 5355–5372.

Wilby R L, Dawson C W, Barrow E M. 2002. SDSM—a decision support tool for the assessment of regional climate change impacts. Environmental Modelling Software, 17(2): 145–157.

Wilby R L, Dawson C W. 2013. The statistical downscaling model: insights from one decade of application. International Journal of Climatology, 33(7): 1707–1719.

Worku M A, Feyisa G L, Beketie K T. 2022. Climate trend analysis for a semi-arid Borana zone in southern Ethiopia during 1981–2018. Environmental Systems Research, 11: 2, doi: 10.1186/s40068-022-00247-7.

Yang C L, Wang N L, Wang S J. 2017. A comparison of three predictor selection methods for statistical downscaling. International Journal of Climatology, 37(3): 1238–1249.